Human Operator Identification in the LPV System Framework

R.F.M. Duarte
ricardo.f.m.duarte@ist.utl.pt

Instituto Superior Técnico, Lisboa, Portugal

November 2016

Abstract

Human interaction with time-varying systems is commonplace these days. Driving a car or piloting an aircraft are examples of such human-machine interactions, where the human operator must adapt his control strategy to the changing dynamics of the system. However, changes in control dynamics of the human operator may also be induced by internal factors, namely fatigue, boredom or even a sudden scare. Therefore, the search for a suitable method that can correctly and sharply identify these changes in the operator dynamics is of the highest importance. In this work, a novel application of the Linear Parameter Varying (LPV) framework to the human operator in single-loop time-varying tracking tasks and subsequent time-varying identification with a Predictor-Based Subspace Identification (PBSID) algorithm is tested. Additionally, two experimentally determined Scheduling Functions, derived from the measured output of the human operator, are tested regarding their model identification performance. A simulation analysis with offline testing based on a recent experimental study was setup and the PBSID algorithm was used to identify the human operator model in different conditions. The results obtained from offline Monte Carlo simulations show good overall model identification, but high noise realization sensitivity. The results further show the possibility of increased freedom in human operator parameter evolution over time when using the LPV framework. An experimental Scheduling Function obtained from zero-phase filtering the second derivative of the human operator output signal was found to capture the time-variation in human operator dynamics, with equivalent accuracy as obtained with analytical Scheduling Functions.
Keywords: LPV, PBSID, time-varying identification, human-machine, scheduling variable

1. Introduction

When controlling complex machinery such as an aircraft, the human operator must constantly employ the best control strategy at a given instant. This strategy emerges from the need to correct the behaviour of the aircraft by interacting with its inputs: a human-machine interaction, where the human operator effectively acts as an in-the-loop controller of the aircraft. Therefore, it is of paramount importance to mathematically model the pilot as a dynamic system, not only to understand and try to predict its response in familiar or unforeseen situations, but also to enhance its training and improve the quality of flight simulator facilities.

The very beginnings of human-machine interaction studies may be traced to the work developed by McRuer et al. [2, 7]. Ever since, extensive research has been done on the identification of the human operator in-the-loop, in both simple single-channel and complex multi-channel tracking tasks [8, 11, 13, 17], in most cases with constant controlled element dynamics. An increased interest in time-varying modeling of the human operator has been emerging, supported on the reasoning that in real-life situations very frequently the human operator needs to adapt himself, either due to a controlled element dynamics that changes over time [20, 21] (for example, an aircraft that stalls, or suffers structural damage), or simply due to accumulated fatigue, momentary distractions or even the boredom experienced while performing a task.

Numerous time-varying identification techniques have been proposed and previously tested, not only for human-in-the-loop identification purposes, but also for industrial-oriented applications [3, 5, 6, 9, 15, 16, 19, 22]. Within the human in-the-loop framework, recursive least-squares, maximum likelihood and wavelet transform analysis algorithms have been implemented [5, 9, 15, 22]. On the other hand, the Linear Parameter-Varying (LPV) system class has been successfully studied and applied for the identification of time-varying behavior of industrial systems [3, 6, 16, 19]. An LPV model assumes the system dynamics change over time and depend exclusively on measurable external variables, called Scheduling Variables. A promising example

of an LPV system identification technique is the Predictor-Based Subspace Identification (PBSID) algorithm, developed and optimized by Chiuso and Van Wingerden et al. [1, 18], and having already been applied for wind turbine LPV identification, with encouraging results. [19]

The innovative use of the LPV framework to identify time-varying human neuromuscular admittance dynamics for steering tasks using the grip force on the steering wheel as Scheduling Variable has recently yielded promising results [12]. However, LPV framework application and subsequent identification of the human in-the-loop operator in aeronautical tracking tasks is still fairly unexplored territory, as selecting an appropriate[1] Scheduling Variable in this context is not a trivial problem.

Most recently, Zaal used a genetic MSE algorithm to identify the adaptation of test subjects to changing controlled element dynamics [20]. However, the assumption that the human operator dynamics change according to the same function that defines the controlled element dynamics change limits the potential for capturing possible non-mapped details and nuances in the evolution of the operator dynamics over time. Due to its reliance on an explicit and possibly experimental Scheduling Variable, the LPV framework could provide an increased freedom in human operator identification, by not requiring strict assumptions on the time-variation of the parameters of the human operator.

The goal of this work thus is to assess the viability of adapting and applying the LPV framework and PBSID algorithm to the time-varying human operator identification problem.

Therefore, this work has the following structure. In Section 2, the fundamental mathematical basis of the PBSID algorithm is described. Section 3 introduces the Zaal setup and offline testing conditions that are used to achieve the goal of the paper. In Section 4, the results of the PBSID algorithm tunning and offline Monte Carlo simulations for all testing conditions are presented and discussed. Finally, the relevant conclusions are presented in Section 5.

2. Background - The PBSID algorithm

The chosen algorithm for the identification of the human operator LPV model is the Predictor-Based Subspace Identification (PBSID) [19]. This section briefly explores its mathematical fundamentals. The following description is based on Refs. 19 and 18.

A Linear Parameter-Varying (LPV) system state-space model with parameter-independent output equation may be modeled by Eq.(1).

$$x_{k+1} = \sum_{i=1}^{m} \mu_k^{(i)} \left(A^{(i)} x_k + B^{(i)} u_k + K^{(i)} w_k \right) \quad (1a)$$

$$y_k = C x_k + D u_k + w_k \quad (1b)$$

where k represents the discrete time unit and m is the number of considered Scheduling Variables; $x_k \in \Re^n$, $u_k \in \Re^r$ and $y_k \in \Re^l$ are, respectively, the state, input and output vectors. The matrices $A^{(i)} \in \Re^{n\times n}$, $B^{(i)} \in \Re^{n\times r}$, $C \in \Re^{l\times n}$, $D \in \Re^{l\times r}$ and $K^{(i)} \in \Re^{n\times l}$ are, respectively, the dynamics, input, output, feedthrough and error intensity matrices. The vector $\mu^{(i)} \in \Re$ is the Scheduling Function (SF), and is comprised of the timed samples k of the i^{th} Scheduling Variable (SV). The white innovation process, $w_k \in \Re^l$, has zero mean and accounts for the error committed when approximating the output y_k with its prediction $\hat{y}_k$, in a one step ahead predictor framework (Eq.(2)).

$$x_{k+1} = \sum_{i=1}^{m} \mu_k^{(i)} \left(\tilde{A}^{(i)} x_k + \tilde{B}^{(i)} u_k + K^{(i)} y_k \right) \quad (2a)$$

$$y_k = C x_k + D u_k + w_k \quad (2b)$$

where $\tilde{A}^{(i)} = A^{(i)} - K^{(i)} C$ and $\tilde{B}^{(i)} = B^{(i)} - K^{(i)} D$.

The main goal of the algorithm is to introduce a factorization which separates the to-be-identified system matrices from the to-be-assumed scheduling sequence. Before achieving it, however, some definitions need to be introduced:

- **The extended time-varying controllability matrix**

  The transition matrix for discrete-time time-varying systems may be defined as in Ref. 14:

  $$\phi_{p,k} = \tilde{A}_{k+p-1} \ldots \tilde{A}_{k+1} \tilde{A}_k \quad (3)$$

  where p is defined as the past window of collected data.

  Using Eq.(3), and grouping the matrices $\tilde{B}$ and K as $\breve{\mathrm{B}}_k = \begin{bmatrix} \tilde{B}_k & K_k \end{bmatrix}^T$, $\bar{B}^{(i)} = \begin{bmatrix} \tilde{B}^{(i)} & K^{(i)} \end{bmatrix}$, the extended time-varying controllability matrix is defined as:

  $$\bar{\mathcal{K}}_k^p = [\left(\phi_{p-1,k+1} \breve{\mathrm{B}}_k \right), \ldots, \left(\phi_{1,k+p-1} \breve{\mathrm{B}}_{k+p-2} \right), \left(\breve{\mathrm{B}}_{k+p-1} \right)] \quad (4)$$

- **The extended time-invariant controllability matrix**

[1] Accurate, low-noise and sensitive to changes in system dynamics.

The operator $\mathcal{L}$ is introduced, which allows for the systematic multiplication of matrices $\tilde{A}$ and $\bar{B}$, in permutations:

$$\mathcal{L}_1 = \begin{bmatrix} \bar{B}^{(1)}, & \dots, & \bar{B}^{(m)} \end{bmatrix} \tag{5}$$

$$\mathcal{L}_p = \begin{bmatrix} \tilde{A}^{(1)}\mathcal{L}_{p-1}, & \dots, & \tilde{A}^{(m)}\mathcal{L}_{p-1} \end{bmatrix} \tag{6}$$

where m represents the number of SVs. Using this operator, the LPV extended time-invariant controllability matrix may be constructed (Eq.(7)).

$$\mathcal{K}^p = \begin{bmatrix} \mathcal{L}_p, & \mathcal{L}_{p-1}, & \dots, & \mathcal{L}_1 \end{bmatrix} \tag{7}$$

- **The Scheduling matrix**

  The Scheduling matrix $\mathcal{N}$ is introduced, aggregating the scheduling sequence within the range of the past window p:

$$\mathcal{N}_k^p = \begin{bmatrix} \mathcal{P}_{p|k} & & & 0 \\ & \mathcal{P}_{p-1|k+1} & & \\ & & \ddots & \\ 0 & & & \mathcal{P}_{1|k+p-1} \end{bmatrix} \tag{8}$$

  where $\mathcal{P}_{p|k} = \mu_{k+p-1} \otimes \mu_{k+p-2} \otimes \cdots \otimes \mu_k \otimes I$, and $\otimes$ represents the Kronecker matrix product.

Finally, the desired factorization of the time-varying extended controllability matrix is achieved:

$$\bar{\mathcal{K}}_k^p = \underbrace{\mathcal{K}^p}_{\text{unknown}} \cdot \overbrace{\mathcal{N}_k^p}^{\text{known}} \tag{9}$$

Note that $\mathcal{K}^p$ depends on the unknown system matrices and $\mathcal{N}_k^p$ depends exclusively on the known scheduling sequence. Consequently, the state equation for the modelled states may now be written as:

$$x_{k+p} = \phi_{p,k}x_k + \underbrace{\mathcal{K}^p\mathcal{N}_k^p}_{\bar{\mathcal{K}}_k^p}\bar{z}_k^p \tag{10}$$

where $\bar{z}_k^p = \begin{bmatrix} z_k & z_{k+1} & \dots & z_{k+p-1} \end{bmatrix}^T$ and $z_k = \begin{bmatrix} u_k^T & y_k^T \end{bmatrix}^T$. If the system is uniformly exponentially stable, $\phi_{j,k} \approx 0$ for all $j > p$, as the influence of the transition matrix outside the considered past window is assumed to be negligible. This approximation becomes perfect for $p \to \infty$, but might result in biased estimates for finite p [19]. Consequently:

$$x_{k+p} \approx \mathcal{K}^p\mathcal{N}_k^p\bar{z}_k^p \tag{11a}$$

$$y_{k+p} \approx C\mathcal{K}^p\mathcal{N}_k^p\bar{z}_k^p + Du_{k+p} + w_{k+p} \tag{11b}$$

Now, the known data is stacked in matrices:
$\mathcal{U}_i = \begin{bmatrix} u_{p+i}, & \dots, & u_{N-f+i+1} \end{bmatrix}$,
$\mathcal{Y}_i = \begin{bmatrix} y_{p+i}, & \dots, & y_{N-f+i+1} \end{bmatrix}$,
$\mathcal{Z}_i = \begin{bmatrix} \mathcal{N}_0^{p+i}\bar{z}_0^{p+i}, & \dots, & \mathcal{N}_{N-p-f}^{p+i}\bar{z}_{N-p-f}^{p+i} \end{bmatrix}$.

If the matrix $\begin{bmatrix} \mathcal{Z}^T & \mathcal{U}^T \end{bmatrix}^T$ has full rank the following linear regression may be solved, to estimate $C\mathcal{K}^{p+i}$ and D:

$$\min_{C\mathcal{K}^{p+i},D} \parallel \mathcal{Y}_i - \left(C\mathcal{K}^{p+i}\mathcal{Z}_i + D\,\mathcal{U}_i\right) \parallel^2 \tag{12}$$

However, the state sequence cannot be directly estimated. So, firstly the extended observability matrix is constructed:

$$\Gamma^F = \begin{bmatrix} C \\ C\tilde{A}^{(i)} \\ \vdots \\ C\left(\tilde{A}^{(i)}\right)^{F-1} \end{bmatrix} \tag{13}$$

where F denotes the future window of predicted data. The product of the extended observability and controllability matrices is then computed (Eq.(14)) using Eq.(13), relation Eq.(15) and the estimation of $C\mathcal{K}^{p+i}$, previously obtained solving Eq.(12).

$$\Gamma^F\mathcal{K}^p = \begin{bmatrix} C\mathcal{L}_p & \cdots & C\mathcal{L}_1 \\ C\tilde{A}^{(1)}\mathcal{L}_p & \cdots & C\tilde{A}^{(1)}\mathcal{L}_1 \\ \vdots & \ddots & \vdots \\ C\left(\tilde{A}^{(1)}\right)^{F-1}\mathcal{L}_p & \cdots & C\left(\tilde{A}^{(1)}\right)^{F-1}\mathcal{L}_1 \end{bmatrix} \tag{14}$$

$$C\mathcal{K}^p = \begin{bmatrix} C\mathcal{L}_p, & C\mathcal{L}_{p-1}, & \dots, & C\mathcal{L}_1 \end{bmatrix} \tag{15a}$$

$$C\mathcal{L}_p = \begin{bmatrix} C\tilde{A}^{(1)}\mathcal{L}_{p-1}, & \dots, & C\tilde{A}^{(m)}\mathcal{L}_{p-1} \end{bmatrix} \tag{15b}$$

The extended observability matrix multiplied by the state sequence ($\Gamma^F\mathcal{K}^p\mathcal{Z}$) is then computed, and the state sequence $\hat{X} = \mathcal{K}^p\mathcal{Z}$ is estimated by performing a Singular Value Decomposition:

$$\widehat{\Gamma^F\mathcal{K}^p}\mathcal{Z} = \begin{bmatrix} \mathcal{W} & \mathcal{W}_\perp \end{bmatrix} \begin{bmatrix} \Sigma_N & 0 \\ 0 & \Sigma \end{bmatrix} \begin{bmatrix} \mathcal{V} \\ \mathcal{V}_\perp \end{bmatrix} \tag{16}$$

where Σ_N denotes a diagonal matrix containing the N largest singular values and $\mathcal{V}$ are the corresponding singular vectors. By selecting only the largest singular values, a reduced number of N states can be estimated:

$$\hat{X}_r = \Sigma_N\mathcal{V} \tag{17}$$

Since the states, the input, the output, the feedthrough and the scheduling sequence are now

known, the remaining system matrices can be determined from Eq.(1).

While the LPV model structure and PBSID algorithm have been successfully used for the identification of wind turbines [18, 19], this paper focuses on their usage for the purpose of human operator identification in a simple single-axis tracking task in an aeronautical context.

3. Implementation

3.1. Tracking Task

The manual control scenario which serves as the basis for the identification algorithm testing is that presented in Ref. 20, with minor adjustments to better fit the purpose of LPV algorithm testing. The block diagram of the pitch control task used to obtain the identification data is shown in Figure 1.

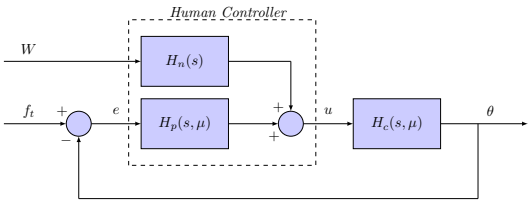

Figure 1: The pitch control task used for testing.

The simplified aircraft pitch dynamics (H_c) and the linear human operator controller and neuromuscular dynamics (H_p) are assumed to have time-varying parameters according to a predefined Scheduling Variable μ, while the human operator remnant filter (H_n) is assumed to be time-invariant. Furthermore, f_t represents the used sinusoidal forcing function and W is a pseudo-white noise signal.

3.2. Scheduling Function

In Ref. 20, the time-varying parameters of H_c and H_p were changed over time according to the sigmoid function:

$$P(t) = P_1 + \frac{P_2 - P_1}{1 + e^{-G(t-M)}} \tag{18}$$

where P_1 represents the initial value of the generic parameter P and P_2 its final value. G is the maximum rate of change of the parameter and M is defined as the time (in seconds) at which it occurs.

For testing purposes, this sigmoid function was defined as the reference analytical scheduling function μ_{A_1}, by introducing the following relation:

$$\begin{aligned} \mu_{A_1}(t) = \frac{1}{1 + e^{-G(t-M)}} \quad \Longrightarrow \\ P(t) = P_1 + (P_2 - P_1) \cdot \mu_{A_1}(t) \end{aligned} \tag{19}$$

where μ_{A_1} denotes, from now on, the reference analytical Scheduling Function within the LPV framework. Fixed $G = 0.5\ s^{-1}$ and $M = 50\ s$ were used. The corresponding time variation of μ_{A_1} is represented in Figure 2.

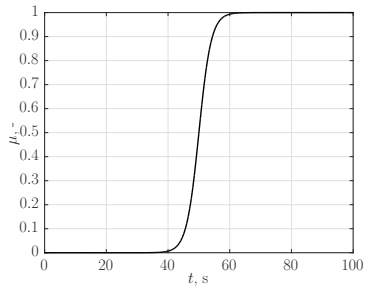

Figure 2: The sigmoid scheduling function μ_{A_1}, used for reference testing purposes.

3.3. Controlled System Dynamics

The controlled dynamics, represented in Figure 1 as H_c, is defined by the transfer function:

$$H_c(s,\mu) = \frac{K_c(\mu)}{s^2 + \omega_b(\mu)s} \tag{20}$$

where both the break frequency w_b and the static gain K_c change over time according to the relation presented in Eq.(19). The initial and final parameter values were set according to Ref. 20.

3.4. Linear Human Operator Dynamics

According to the human operator model developed by McRuer et al. [7], the human operator is expected to close the loop in a way that the closed-loop frequency response approximates that of a single-integrator system, around the crossover frequency. In this case, the human operator compensation dynamics is expected to be mostly a gain in the early stages of the simulation, and both a gain and a lead component in the later stages of the simulation: a result verified in Ref. 20.

Hence, for the linear human operator model H_p, a time-varying visual gain K_v, a time-varying first-order term K_s, a constant visual delay τ_v and neuromuscular limitations ω_{nm} and ζ_{nm} are assumed, as shown in Eq.(21). [20]

$$\begin{aligned} H_p(s,\mu) = [K_s(\mu)s + K_v(\mu)] \cdot e^{-s\tau_v} \\ \times \frac{\omega_{nm}^2}{s^2 + 2\zeta_{nm}\omega_{nm}s + \omega_{nm}^2} \end{aligned} \tag{21}$$

where both K_v and K_s change over time according to Eq.(19), with initial and final conditions according to the results obtained by Zaal [20].

3.5. Non-Linear Human Operator Dynamics

The non-linear human operator dynamics was simulated by having a pseudo-white noise signal W passing through a low-pass remnant filter H_n. This filter

was defined as $H_n = K_n/(0.2s+1)$, and the gain K_n was chosen so that the power of the remnant signal in the initial single-integrator dynamics phase of the simulation, $P_n = \sigma_n^2/\sigma_u^2$, is as desired. Since no time variation of K_n is assumed, a lower remnant signal power towards the end of the simulation ensues, as the controlling activity increases. The resulting filtered white-noise signal is then added to the linear response of the human operator, to produce its output u.

3.6. Scheduling Function Tests

In the LPV framework, the Scheduling Function is critical, as it directly drives the time variation of the modelled system dynamics. [18]. For the LPV identification of a human controller, a suitable, measurable Scheduling Variable must be found, so that a Scheduling Function that reflects the change in dynamics of the human operator can be constructed.

Therefore, the Scheduling Function tests focus on comparing different Scheduling Functions regarding their performance on the identification of the LPV model, with data collected from Monte Carlo runs of 100 noise realizations each, and with respect to three regions of interest (Figure 3).

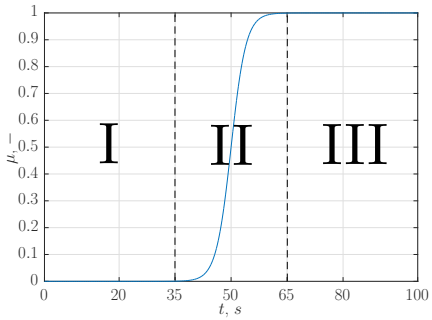

Figure 3: The three regions of testing assessment, with μ represented.

In Region I, the human operator equalization is predominantly a gain; Region II is the transition region; in Region III, the human operator dynamics is the combination of a gain and lead compensation.

As Region II is the crucial transition phase in between dynamics, the VAF and Correlation between Scheduling Functions results were obtained for the full simulation and for the transition Region II. The parameter estimation bias results were obtained for all of the regions (I - III).

Four Scheduling Functions were selected for testing: two of analytical origin (μ_A) and two of experimental origin (μ_E).

- **Analytical Scheduling Function** μ_{A_1} (Figure 4(a)) is the reference Scheduling Function, previously defined in Section 3-3.2.
- **Analytical Scheduling Function** μ_{A_2} (Figure 4(a)) consists on the Scheduling Function μ_{A_1} with a "perturbation" added to it. This perturbation is a Gaussian curve with average at 50 seconds, standard deviation of eight seconds and amplitude of 0.6.
- **Experimental Scheduling Function** μ_{E_1} (Figure 4(c)) is based on the second derivative of the human operator output, $\ddot{u}$. Figure 4(b) indicates that $\ddot{u}$ might hold crucial information about the evolution of the human operator system dynamics over time. However, to be usable as a Scheduling Function, the raw data of $\ddot{u}$ had to undergo some post-processing. Here, $\ddot{u}$ was treated with successive RMS filterings [4], where a movable filtering window ten samples wide was used. The high amount of RMS filtering was necessary to guarantee the usability of μ_{E_1} as Scheduling Function, specially in high human operator remnant conditions. Afterwards, the filtered $\ddot{u}$ was normalized, to ensure a fair comparison between Scheduling Functions.
- **Experimental Scheduling Function** μ_{E_2} (Figure 4(c)) treats $\ddot{u}$ with a zero-phase digital filtering, processing the data with a linearly optimized Butterworth low-pass filter in both forward and reverse directions. [10] The optimization process makes use of a cost function which compares the resulting μ_{E_2} with the corresponding experimental Scheduling Function μ_A and strives to minimize the error by tweaking the filter coefficients.

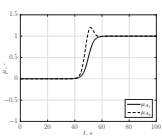

(a) The analytical Scheduling Functions μ_{A_1} and μ_{A_2}.

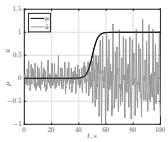

(b) μ_{A_1} and $\ddot{u}$ over time. The change in control activity coincides with the change in dynamics.

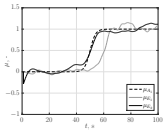

(c) Time traces of μ_{E_1} and μ_{E_2}, for a single realization with $P_n = 0.05$.

Figure 4: Analytical and experimental Scheduling Functions.

The four Scheduling Functions were tested by performing the identification of H_p for two different conditions:

- **Condition** $\bar{P}$**:** without the Gaussian perturbation in H_p parameters K_v and K_s.
- **Condition** P**:** The same Gaussian curve that is included in μ_{A_2} is added to K_v and K_s.

Table 1 compiles the testing conditions. A consequence of this setup is that the Scheduling Function μ_{A_1} serves as the reference for the H_p condition $\bar{P}$, while μ_{A_2} is the reference for condition P.

Table 1: Scheduling Function testing conditions.

H_p Condition	Scheduling Function			
	Analytical		**E**xperimental	
	μ_{A_1}	μ_{A_2}	μ_{E_1}	μ_{E_2}
$\bar{P}$	$\bar{P}_{A_1}$	$\bar{P}_{A_2}$	$\bar{P}_{E_1}$	$\bar{P}_{E_2}$
P	P_{A_1}	P_{A_2}	P_{E_1}	P_{E_2}

4. Results

The results obtained in this section are based on the models obtained using $F = N = 2$ and $p = 120$ as PBSID settings.

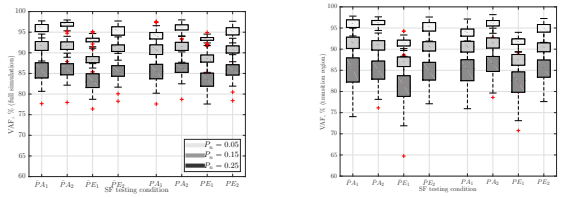

(a) Full simulations. (b) Region II.

Figure 5: VAF of identified reduced models, for different SF conditions and $P_n = 0.05$, 0.15 and 0.25.

Figure 5(a) represents the distribution of the VAF values attained in the Monte Carlo runs for the different SF and P_n conditions. For no H_p perturbation conditions ($\bar{P}$), the SF μ_{A_1} yields the highest VAF values for every P_n level bar $P_n = 0.05$, being the reference SF for this condition. Remarkably, the SF μ_{E_2} presents very similar results for every P_n value, providing good indications about the usefulness of this experimental SF in the identification process. The SF μ_{A_2} is very similar to μ_{A_1}, the difference being the addition of the perturbation in Region II. As such, the results are quite similar between the two analytical SFs, with both obtaining quite similar scores for condition $\bar{P}$ and μ_{A_2} obtaining higher scores for condition P, where μ_{A_2} is the reference. The VAF values of the models identified with μ_{E_1} are generally lower than with μ_{E_2}, for both conditions. These trends are maintained throughout Region II (Figure 5(b)), but the differences between μ_{A_1}, μ_{A_2} and μ_{E_1}, μ_{E_2} are now more pronounced. In fact, this is a critical region: the perturbation that differentiates μ_{A_1} and μ_{A_2} is defined in this region, and the penalization of using an unsuitable SF for identification is clearly visible. Regarding the experimental SFs, the heavy RMS filtering needed to make $\ddot{u}$ usable as an experimental SF introduces a delay in μ_{E_1}, which is most clearly perceptible in Region II. This in turn accentuates the VAF difference between μ_{E_1} and μ_{E_2} in this region and fleshes out the dangers of phase-altering filtering Scheduling Functions.

Figure 6 further explores the comparison between the experimental Scheduling Functions by showing their correlation with the respective reference analytical SF, for different P_n levels. It is perceptible that for every condition, μ_{E_2} is better correlated with either μ_{A_1} or μ_{A_2} than μ_{E_1}. Furthermore, the correlation values concerning μ_{E_2} are consistently above 0.9, a value μ_{E_1} only seldom achieves. It is also noticeable a general trend for the correlation to decrease as the condition changes from $\bar{P}$ to P, which suggests both experimental SFs have some trouble detecting small perturbations in the human operator dynamics. Focusing on Region II, it is possible to observe a high correlation variance concerning μ_{E_1}, which indicates a severe lack of consistency. When comparing the results of the full simulation with those of Region II, a general drop in correlation becomes apparent. This drop is strong for μ_{E_1}, due to its relative delay; it is, however, much smaller for μ_{E_2}, further evidencing the superior SF quality of μ_{E_2} over μ_{E_1}.

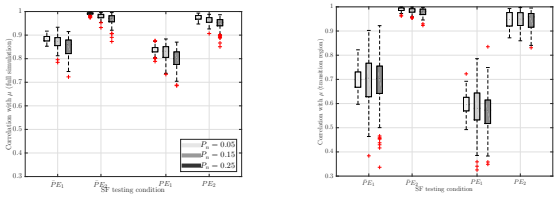

(a) Full simulations. (b) Region II.

Figure 6: Correlation of experimental SFs with their analytical counterparts, for different SF conditions and $P_n = 0.05$, 0.15 and 0.25.

Through analysis of Figures 7(a)-(c), it is possible to observe a much more accurate K_v estimation for all testing conditions in Region I when compared with Region III. In fact, the absolute value of the normalized bias for Region I is rarely above 20%, even for $P_n = 0.25$. On the other hand, Region III K_v estimations seem to be worse, with some runs of $P_n = 0.25$ achieving a normalized bias as high as 80%. Throughout the different testing regions, a distinct tendency for undershooting the estimation of K_v is present, as evidenced by the median of the normalized biases of the different conditions. Finally, there is not much difference in K_v estimation between the considered SFs, apart from a slightly worse performance of μ_{E_1} in Regions I and II. Analysing these plots with the help of Figure 5, it may be concluded that the parameter K_v has rela-

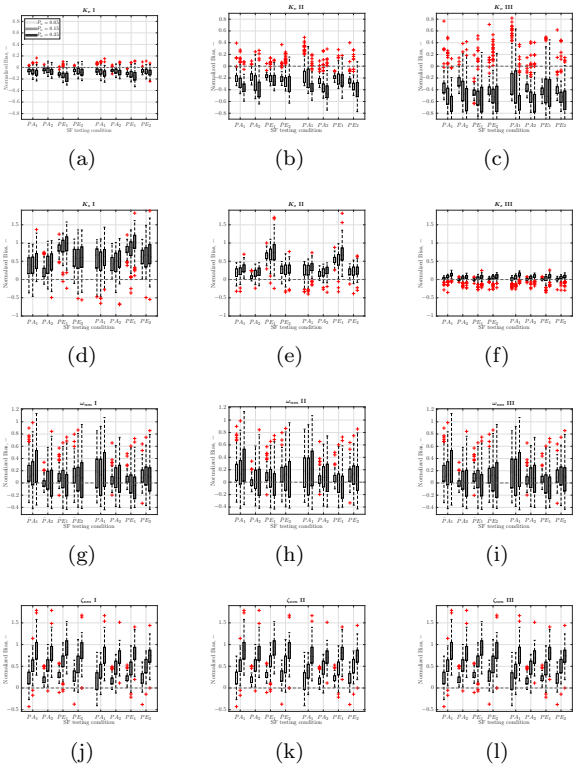

Figure 7: Bias in parameter estimation, for different regions and $P_n = 0.05$, 0.15 and 0.25.

tively small influence in the estimated overall model quality.

In turn, the subsequent trio of sub-figures (Figures 7(d)-(f)) presents much more conclusive results regarding the fundamental differences in VAF witnessed in Figure 5. In fact, the K_s estimation using μ_{E_1} proves to be worse than with μ_{E_2}, especially concerning Regions I and II. This result combined with Figure 5 indicates that, in the considered framework, the lead term K_s is more important than K_v in obtaining good-fitting models. There is not a significant difference in estimation bias between different human operator remnant intensities, and the overall bias reduces in Region III, evidencing very good performance in K_s estimation for this particular region.

Figures 7(g)-(i) concern ω_{nm}, which is supposed to be non time-varying. Accordingly, the normalized bias results are the same throughout the different regions. A very high variance is observed, with a tendency to overshoot the real value. This unusually high variance contributes to a lack of ω_{nm} estimation precision, and gets worse as P_n increases. No significant differences between SFs or H_p conditions are detected.

For ζ_{nm}, Figures 7(j)-(l) show no bias variation between regions, as expected. However, much like ω_{nm}, the normalized bias variance is still very high. As P_n increases, the estimation gets gradually worse, and there are no significant differences between SFs or H_p conditions.

These results collectively reveal the potential of $\ddot{u}$ to be used as an experimental Scheduling Function, by carefully filtering the high-frequency oscillations. A phase-shifting filtering method, like RMS, was shown to be especially problematic in Region II, where the dynamics transition occurs. The zero-phase filtering of $\ddot{u}$ (μ_{E_2}) presented better VAF results, in both the full simulation and Region II, yielding estimated models with very close VAF values to the ones generated by the analytical sigmoid-based SFs. However, both experimental SFs fail to accurately capture the perturbation introduced for condition P, as evidenced by the decrease in SF correlation for this condition (Figure 6).

Additionally, the parameter estimation bias is generally higher than that obtained in Ref 20 and a high number of parameter estimates turned out to be outliers, which shows the high-sensibility nature of the algorithm to different noise realizations. A possible solution to this problem might be averaging the identification data of the Monte Carlo runs, so that the human operator remnant is diluted and reduced.

5. Conclusions

This work had the goals of assessing the viability of using the LPV framework and the PBSID algorithm to solve the time-varying human in-the-loop identification problem, and to find a suitable experimental Scheduling Variable that can be used for the LPV identification. To accomplish this, an offline recreation of the experiment in Ref 20 was used as a testing bed. Monte Carlo runs with representative human operator remnant noise realizations were performed, and the human operator dynamics was identified as an LPV model using the PBSID algorithm, with different testing conditions and Scheduling Functions. The identified models were compared using VAF and the relative bias of the model parameters. The comparison between analytical and experimental Scheduling Functions yielded encouraging results regarding the Scheduling Function obtained from zero-phase filtering the second derivative of the human operator output signal (μ_{E_2}). In fact, the models identified with this experimental SF produced VAF values very close to the models identified with the analytical Scheduling Functions for condition $\bar{P}$ (no perturbation in H_p dynamics). Furthermore, for condition P (perturbation in H_p dynamics), the μ_{E_2} models had slightly higher VAF values than the models obtained through the reference analytical SF taken from Ref. 20, which represents an improvement.

Future work in the application of the LPV framework for the identification of the human operator

in tracking tasks may be developed. Experimental data testing using the time-varying controlled element of Ref. 20 and human test subjects to validate μ_{E_2} as a suitable SF for LPV identification is a natural continuation to the work developed in this paper. Within the PBSID algorithm, a thorough analysis on the effects of the p and F in model estimation quality would add a more precise understanding on the optimal PBSID settings for the specific application presented in this paper. The key aspect of the LPV framework lies in the Scheduling Variable. Therefore, a research on suitable candidate Scheduling Variables to be used for time-varying human operator identification in tracking tasks is of high importance. An interesting research topic also lies on the possibility of using multiple Scheduling Variables for LPV identification, and their effects on model quality and parameter estimation.

References

[1] A. Chiuso. The role of vector autoregressive modeling in predictor-based subspace identification. *Automatica*, 43(6):1034 – 1048, 2007.

[2] R. E. Duane T. McRuer and G. P. Moore. A neuromuscular actuation system model. *IEEE Transactions on Man-Machine Systems*, MMS-9(3), sep 1968.

[3] L. Giarr, D. Bauso, P. Falugi, and B. Bamieh. Lpv model identification for gain scheduling control: An application to rotating stall and surge control problem. *Control Engineering Practice*, 14(4):351 – 361, 2006.

[4] IEEE. Standard on transitions, pulses, and related waveforms, 2003.

[5] M. Kers. Maximum Likelihood Estimation of Linear Time-Varying Pilot-Vehicle System Parameters. Master's thesis, Delft University of Technology, Aug. 2012.

[6] G. M. M. Lovera and E. Laroche. Identification of a flexible robot manipulator using a linear parameter-varying descriptor state-space structure. In *50th IEEE Conference on Decision and Control and European Control Conference (CDC-ECC)*, 2011.

[7] D. T. McRuer and H. R. Jex. A review of quasi-linear pilot models. *IEEE Transactions on Human Factors in Electronics*, HFE-8(3), sep 1967.

[8] F. M. Nieuwenhuizen, P. M. T. Zaal, M. Mulder, M. M. van Paassen, and J. A. Mulder. Modeling Human Multichannel Perception and Control Using Linear Time-Invariant Models. *Journal of Guidance, Control, and Dynamics*, 31(4):999–1013, July-August 2008.

[9] M. Olivari, F. M. Nieuwenhuizen, H. H. Bülthoff, and L. Pollini. Identifying Time-Varying Neuromuscular System with a Recursive Least-Squares Algorithm: a Monte-Carlo Simulation Study. In *Proceedings of the 2014 IEEE International Conference on Systems, Man, and Cybernetics, San Diego (CA)*, pages 3573–3578, Oct. 2014.

[10] A. V. Oppenheim, R. W. Schafer, and J. R. Buck. *Discrete-Time Signal Processing*. Upper Saddle River, NJ, 1999.

[11] D. M. Pool. Pilot Control in Compensatory Roll Axis Tracking Tasks. Master's thesis, Delft University of Technology, 2007.

[12] A. Pronker. Estimating time-varying neuromuscular admitance during steering tasks (preliminary msc. thesis). Master's thesis, Faculty of Aerospace Engineering - Delft University of Technology, 2015.

[13] N. Roggenkämper, D. M. Pool, F. M. Drop, M. M. van Paassen, and M. Mulder. Objective ARX Model Order Selection for Multi-Channel Human Operator Identification. In *Proceedings of the AIAA Modeling and Simulation Technologies Conference, Washington, D.C.*, number AIAA-2016-4299, June 2016.

[14] W. Rugh. *Linear system theory*. Upper Saddle River, 1996.

[15] P. M. Thompson, D. H. Klyde, and M. J. Brenner. Wavelet-Based Time-Varying Human Operator Models. In *Proceedings of the AIAA Atmospheric Flight Mechanics Conference and Exhibit, Montreal (CA)*, number AIAA-2001-4009, 2001.

[16] R. Tóth, V. Laurain, M. Gilson, and H. Garnier. Instrumental variable scheme for closed-loop LPV model identification. *Automatica*, 48:2314–2320, 2012.

[17] K. van der El, D. M. Pool, H. J. Damveld, M. M. van Paassen, and M. Mulder. An Empirical Human Controller Model for Preview Tracking Tasks. *IEEE Transactions on Cybernetics*, 2015.

[18] J. van Wingerden and M. Verhaegen. Subspace identification of bilinear and lpv systems for open and closed loop data. *Automatica*, 45(2):372–381, 2009.

[19] J. W. van Wingerden. *Control of Wind Turbines with Smart Rotors: Proof of Concept & LPV Subspace Identifcation*. PhD thesis, Technische Universiteit Delft, 2008.

[20] P. M. Zaal. Manual control adaptation to changing vehicle dynamics in rollpitch control tasks. *Journal of Guidance, Control and Dynamics*, 2016.

[21] P. M. T. Zaal and D. M. Pool. Multimodal Pilot Behavior in Multi-Axis Tracking Tasks with Time-Varying Motion Cueing Gains. In *Proceedings of the AIAA Modeling and Simulation Technologies Conference, National Harbor (MD)*, number AIAA-2014-0810, Jan. 2014.

[22] P. M. T. Zaal and B. T. Sweet. Estimation of Time-Varying Pilot Model Parameters. In *Proceedings of the AIAA Modeling and Simulation Technologies Conference, Portland, Oregon, Aug. 8-11*, number AIAA-2011-6474, 2011.